Petroleum Science 21 (2024) 1584–1596

Contents lists available at ScienceDirect

Petroleum Science

journal homepage: www.keaipublishing.com/en/journals/petroleum-science

Original Paper

A regression approach for seismic first-break picking

Huan Yuan [a, b], San-Yi Yuan [a, *], Jie Wu [b], Wen-Jing Sang [a], Yu-He Zhao [b]

[a] CNPC Key Laboratory of Geophysical Exploration, China University of Petroleum (Beijing), Beijing 102249, China
[b] Research Institute of Petroleum Exploration & Development—Northwest (NWGI), Key Laboratory of reservoir characterization of CNPC, PetroChina, Lanzhou 730020, Gansu, China

ARTICLE INFO

Article history:
Received 28 May 2023
Received in revised form
8 September 2023
Accepted 28 November 2023
Available online 4 December 2023

Edited by Jie Hao and Meng-Jiao Zhou

Keywords:
First-break picking
Low signal-to-noise ratio
Regression
BiLSTM
Traveltime
Geometry
Noisy seismic data

ABSTRACT

The picking efficiency of seismic first breaks (FBs) has been greatly accelerated by deep learning (DL) technology. However, the picking accuracy and efficiency of DL methods still face huge challenges in low signal-to-noise ratio (SNR) situations. To address this issue, we propose a regression approach to pick FBs based on bidirectional long short-term memory (BiLSTM) neural network by learning the implicit Eikonal equation of 3D inhomogeneous media with rugged topography in the target region. We employ a regressive model that represents the relationships among the elevation of shots, offset and the elevation of receivers with their seismic traveltime to predict the unknown FBs, from common-shot gathers with sparsely distributed traces. Different from image segmentation methods which automatically extract image features and classify FBs from seismic data, the proposed method can learn the inner relationship between field geometry and FBs. In addition, the predicted results by the regressive model are continuous values of FBs rather than the discrete ones of the binary distribution. The picking results of synthetic data shows that the proposed method has low dependence on label data, and can obtain reliable and similar predicted results using two types of label data with large differences. The picking results of 9380 shots for 3D seismic data generated by vibroseis indicate that the proposed method can still accurately predict FBs in low SNR data. The subsequent stacked profiles further illustrate the reliability and effectiveness of the proposed method. The results of model data and field seismic data demonstrate that the proposed regression method is a robust first-break picker with high potential for field application.

1. Introduction

In exploration seismology, first breaks (FBs) are defined as the moment when the effective seismic wave first arrives at the geophone through the formation. FBs are necessary information in seismic reflection processing. For instance, it is helpful for near-surface velocity estimation and static correction to remove the influence of the weathering layer on seismic imaging, which is the cornerstone of subsequent seismic data processing and interpretation (Yilmaz, 2001). Therefore, it is of great significance to precisely and quickly pick FBs of seismic records.

Manual picking is the most straightforward method. It can introduce any prior knowledge, such as the spatial continuity of the first arrival wave. Even for low-quality or irregular seismic traces, experienced data analysts can still interpret high-quality FBs by utilizing the information of neighborhood traces. However, due to massive amounts of seismic data for the popularization of two wide and one high seismic acquisition (i.e., wide azimuth, wide broadband, and high density), manual picking is very time-consuming and expensive to identify FBs, especially in low signal-to-noise ratio (SNR) seismic data acquired under complex topography and complex underground structure conditions. Moreover, it is easy to generate system errors which usually cannot be eliminated. Therefore, how to identify FBs in extensive and low SNR seismic data efficiently and precisely remains a crucial challenge.

Various (semi-)automated first-break picking methods have been proposed and developed to improve the picking efficiency and to alleviate the pressure of interpreters. Several automatic picking methods have been proposed in the literature, such as energy-based methods (Coppens, 1985; Gaci, 2014), entropy-based methods (Sabbione and Velis, 2010), fractal-based methods (Boschetti et al., 1996; Jiao and Moon, 2000), Akaike information

* Corresponding author.
E-mail address: yuansy@cup.edu.cn (S.-Y. Yuan).

https://doi.org/10.1016/j.petsci.2023.11.028

criterion-based methods (Takanami and Kitagawa, 1991, 1993; Sleeman and Eck, 1999), and higher-order statistics based methods (Yung and Ikelle, 1997; Tselentis et al., 2012). In general, these methods work well on data with strong peak amplitude, stable noise, and consistent waveform. They extract a sensitive property response to FBs, such as fractal dimension, energy, kurtosis etc. (Saragiotis et al., 2004). However, in the case of rough terrains and complex subsurface structures, these methods sometimes have poor performance and suffer from some noise and energy loss.

In contrast to single-trace (semi-)automated methods, multi-trace methods, such as cross-correlation-based methods (Gelchinsky and Shtivelman, 1983; Molyneux and Schmitt, 1999), make use of spatial characteristics of receivers within the array simultaneously. The classical multi-trace-based method determines the FBs by taking maximum values of the cross-correlation or convolution results from trace(s) to trace(s). Due to the simultaneous usage of multiple traces or high-dimension (2D or 3D) seismic data information, the multi-trace-based method can identify weak signals or pick FBs at low SNR (Gibbons and Ringdal, 2006) to some extent when the spatial waveform of seismic waves is relatively consistent. However, they often do not adapt to situations where the waveforms change drastically with the traces and there exist missing traces or bad traces owing to strong noise and rugged topography.

Most single- or multi-trace methods compute only one attribute for each time sample and subsequently select the location with maximum- or minimum-value attributes as FBs. As a rule, it generally does not accurately correspond to the FBs based on these single- or multi-trace methods when noise is heavy or seismic waveform changes dramatically. To improve the stability and accuracy, neural network methods are introduced to extract multiple attributes automatically to classify waveforms and to pick FBs. It is to pick FBs using these methods by statistical criterion (Gelchinsky and Shtivelman, 1983; Akram and Eaton, 2016) or the fully connected neural networks (Gentili and Michelini, 2006; Maity et al., 2014; Khalaf et al., 2018) for extracting multiple dimensionless characteristic parameters or multiple derived attributes from seismic data correspond to FBs. In geophysics, a basic idea is to convert seismic data or attributes into regular images, and then build a network model with deep hidden layers to analyze and extract multiple first-break attributes to identify FBs. It is very time-consuming to identify the arrival times by traditional neural networks at the cost of tremendous amount of manual workload to pick FBs first of all. Moreover, the picking quality of the FBs heavily relied on extracted sensitive attributes, such as amplitude, frequency, instantaneous amplitude and phase, polarity, peak envelope slope, peak amplitude, RMS amplitude ratio, SNR, correlation between adjacent channels, offset, and wavelet (McCormack et al., 1993; Maity et al., 2014).

Convolutional neural networks (CNNs) are utilized to effectively and rapidly detect or classify seismic waveforms and to pick FBs by a spatiotemporal waveform classification involving the images within a sliding window (Yuan et al., 2018). Then it is analyzed the strong importance of label quality in picking FBs. Li et al. (2022, 2023) used CNNs based on computer vision to identify and separate microseismic waveforms. Compared with CNNs, fully convolutional networks (FCNs) can extract local and global features of an image and achieve fine segmentation at the pixel level. The FCNs were developed based on CNNs, and several variants of FCNs including U-net (Ronneberger et al., 2015), DeepLab (Chen et al., 2018), SegNet (Badrinarayanan et al., 2017) and DeconvNet (Noh et al., 2015) have become popular for geophysical exploration in recent years. The surge of artificial intelligence results in novel research hotspots in geophysical exploration, including FBs picking using FCNs (Hu et al., 2019; Zhao et al., 2019; Chen et al., 2020; Zhang and Sheng, 2020; David et al., 2021; Han et al., 2021; Yuan et al., 2022). The key advantage of the abovementioned FCNs is the ability to learn appropriate feature representations in an end-to-end, image-to-image, pixel-to-pixel manner. However, the end-to-end deep learning construction is a black box that is not convenient for real-time quality control. Therefore, some semi-supervised neural networks were developed to pick FBs with human interpretation (Tsai et al., 2020; Duan and Zhang, 2020). We can save a lot of labor and time costs by CNNs and FCNs in seismic data with high SNR. Deep learning (DL) techniques are powerful for high-dimensional classification and have achieved great success in large-scale images owing to extensive labeled databases. The same as other classification tasks, the ultimate efficiency and effectiveness of picking FBs by DL-based methods depend on huge labels that technicians make manually at great expense of time and energy (Saxe et al.). Generally, seismic records are seriously polluted by noise collected under rugged topography and complex underground structures. Making labels strictly meeting the conditions of consistent size, uniform distribution, similar waveforms, and representative features in massive data is extremely time-consuming and labor-intensive work. Therefore, picking FBs based on DL and image segmentation still faces great challenges in industrial applications.

In this paper, after studying the disadvantages of traditional image segmentation and classification based FBs picking in detail, we present a regression approach to directly pick seismic FBs based on geometric seismology, which uses the deep learning network to learn the implicit relationships among the elevation of shots, offset and the elevation of receivers to their seismic travel-time to predict the unknown FBs, from common-shot gathers with sparsely distributed traces.

We begin this paper with an introduction of the motivation and general framework, as well as the description of data preparation, network architecture design, network model training, model update, and the optimum model application. Two seismic datasets including one theoretical model and one 3D field seismic data with 9380 shot gathers with low SNR are then adopted to illustrate the effectiveness of the proposed method from shot gathers. Finally, a discussion and some conclusions are given.

2. Methodology

2.1. First-break picking based on seismic image and waveform classification

FBs refer to the earliest arrival traveling time of seismic waves to receivers in the field of P-wave exploration. Therefore, there is only one first break in each trace. In the shot gather, the above FBs are mainly the environment or background noise with poor correlation, and seismic waveform below the FBs shows obvious correlation in space, and this feature is generally used to pick FBs.

The essence of artificial intelligence picking technology with the concept of image classification is to determine the demarcation moment of the effective signal and environmental noise in seismic data sets, which is specifically manifested in the seismic data volume as the use of neural networks to classify 2D or 3D images. The classification problem of whether the first arrival wave is converted into the classification problem of the background noise above the FBs (pure noise) and the effective signal class below the FBs (signal + noise), which are represented by vectors [0 1] and [1 0], respectively, and the boundary between them is the FBs. The prevalent networks are mainly FCNs and their improved networks

(U-Net and SegNet). After manually labeling the datasets, a series of processes are finally used to determine the first arrival time. However, in exploration areas with complex surface and complex subsurface structures, the following phenomena usually exist in the first arrival waves:

1) The first arrival waves include a variety of different types of waves, such as shallow refracted waves, deep refractive waves, reflected waves, direct waves, contraflexure waves at different depths, etc., generally accompanied by a chaotic phase.
2) There are random interference waves before the first arrival waves and secondary waves with difficulty in recognizing and picking first arrival waveform from features.
3) In general, there is bad spatial consistency of the seismic first arrival waveform, due to random absent traces and irregular field seismic acquisition.
4) There is ambient noise whose frequency and waveform characteristics are different from the first arrival waves. These phases of interferences among traces are highly random, resulting in difficult to track peaks or troughs for the first arrival waves among adjacent traces.

2.2. First-break picking based on geometric seismology and regressive model

The above phenomena make it difficult to accurately and quickly identify the boundary of effective signal and noise by image segmentation in massive low SNR seismic data records.

When seismic waves propagate in a medium, each spatial point has its own traveling time of the wave-front. The traveltime of wave-front t can be seen as a function of spatial position in Euclidean space, noted as $t = g(x_s, x_r)$. It is a function that represents the time it takes for the wave-front to travel from the source point through the medium to any receiver point. The Eikonal equation describes the relationship between the traveltime from the source to the receiver point and the velocity parameter of the 3D subsurface heterogeneous medium (Noack and Clark, 2017). In a medium with complex surfaces and complex subsurface structures, the traveltime equation for the seismic first arrival wave can be expressed as

$$t_r = \mathrm{F}(Vr, Es, Er, O) \tag{1}$$

where t_r is the traveltime of the first arrival wave, F(•) is a nonlinear function, Vr is the velocity of the subsurface medium below the receiver, Es is the elevation of the shot, Er is the elevation of the receiver, and O is the offset from shot to receiver.

From Eq. (1), it can be seen that the FBs only depend on the parameters of the geometry without relying on the seismic data itself by solving the Eikonal equation. Therefore, the issue of picking FBs can be transformed into the regression problem based on geometry parameters, rather than seismic waveform classification on image segmentation.

At this point, the key problem is to identify the nonlinear mapping relationship between the information of geometry and the first arrival wave traveling time by deep neural network. In Cartesian coordinates, for a certain seismic trace, we can build the implicit Eikonal equation Regpicker(•) on the ground of FBs label t_r, the elevation of the shot Es, the elevation of the shot Er and the offset O to predict traveltime t_p at the geophone at the current medium space, described as

$$t_p = \mathrm{Regpicker}(\mathbf{x};\mathbf{w};\mathbf{b}) \tag{2}$$

where $\mathbf{x}$ is a vector consisted of the geometry parameters Es, Er and O, and $\mathbf{w}$ and $\mathbf{b}$ denote weights and biases of deep neural network, respectively. When Regpicker(•) approximates F(•) in Eq. (1), traveltime t_p predicted by the deep neural network approaches the label t_r.

In this paper, the artificial intelligence regression method for picking FBs based on sparsely labeled data from shot gather is presented, which mainly includes data preparation and normalization processing, network frame design, network model evaluation, and application of the optimal model.

2.3. Data preparation

To obtain effective and generalizable trained models or network parameters, it is necessary to prepare three types of seismic data: training set, validation set, and test set. The training set data is used to train the model to obtain optimal network parameters. The validation set is used to evaluate whether the trained network parameters are underfitted or overfit to determine whether the important hyper-parameters selected in the training set are appropriate. If these phenomena occur, the optimal parameters of the network model should be retrained by adjusting the number of hidden layers, the learning rate, the minimum batch size, the maximum number of iterations, and the evaluation function. The test set is considered to investigate the generalization ability of the well-trained model to unseen shot gathers. The data of the training set, validation set, and test set are spatially distributed arbitrarily, and they do not require regularity and continuity. To learn the model stably, fast, and effectively, all samples in different sets should be further preprocessed mainly including normalization, mapping the data into the range of 0–1.

The above three types of set data all include four kinds of data: elevation of receiver, elevation of shot, offset, and FBs. In this paper, the input data $\mathbf{x}$ for the deep neural network are selected as three parameters, elevation of receiver, elevation of shot, and offset. The output data are the vector of FBs arranged in the order of seismic trace. Since the output data is seismic FBs which are randomly and sparsely distributed rather than a regular image, the FBs picked by automatic or manual method can be used as label data to improve the efficiency of making labels. In this paper, the high-order statistical method (Saragiotis et al., 2004; Tselentis et al., 2012) is used to pick FBs first, and then an automatic algorithm is designed to choose reliable FBs as labels. The label doesn't need to be a regular and continuous high-density image, and the data preparation process does not need a series of complex preprocessing work, such as manually picking the FBs, eliminating the anomalous value, surface wave attenuation, filtering, and clipping et al., which is necessary for the CNN-based classification network. For the proposed method, making labels is flexible and efficient, the data preparation process is simple and fast, and we can focus on optimizing network parameters and improving the picking accuracy.

2.4. Long short-term memory network

The models of the traditional recurrent neural network (RNN) will only focus on the processing of information in the current moment and will not infer whether the processing of information in the previous moment will help in the next moment, and the problems of local minima, gradient disappearance, and gradient explosion are prevalent when performing model training. For example, the gradient disappearance generated by RNN during

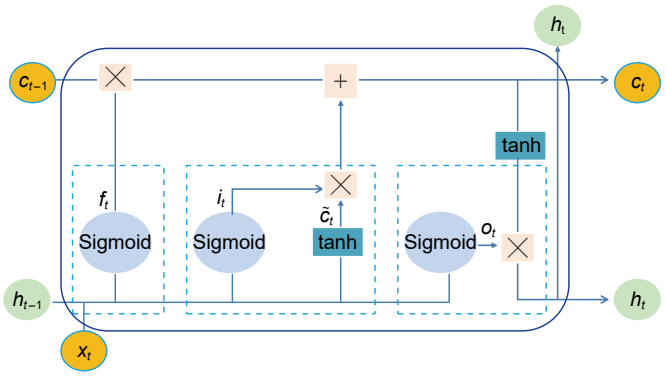

Fig. 1. Internal structure of LSTM.

backpropagation can lead to the inability to capture long-term dependence. Long short-term memory network (LSTM) is a special implementation of RNN. The structure of the LSTM hidden unit is shown in Fig. 1, which improves the implicit layer and introduces the concept of temporal order on top of RNN neural networks so that the output of one moment can have a direct impact on the input of the next moment. In Fig. 1, $\mathbf{x}_t$ represents the input sequence, $\mathbf{h}_t$ represents the output, $\mathbf{c}_t$ represents the cell state at the moment noted by t, and $\tilde{\mathbf{c}}_t$ represents the candidate cell at the moment of t. LSTM uses three types of gating: input gate $\mathbf{i}_t$, forgetting gate $\mathbf{f}_t$, and output gate $\mathbf{o}_t$ to store and update information in long term. The forgetting gate $\mathbf{f}_t$, in the cell state transfer determines what information should be discarded. The input gate $\mathbf{i}_t$ controls the decision of what new information to add to the "cell state". The output gate $\mathbf{o}_t$ controls the storing of the information of the cell at the moment t to the hidden state of $\mathbf{h}_t$. The sigmoid layer determines which values need to be updated, and the tanh layer determines what new values to add.

The input gate $\mathbf{i}_t$ control information updates, and the calculation formula is shown as follows:

$$\mathbf{i}_t = \sigma(\mathbf{W}_i \cdot [\mathbf{h}_{t-1}, \mathbf{x}_t] + \mathbf{b}_i) \tag{3}$$

where σ is a sigmoid function, $\mathbf{W}_i$ is the weight of the input gate, and $\mathbf{b}_i$ is the deviation of the input gate. The forgetting gate $\mathbf{f}_t$ is used to control the forgetting degree of information in cell $\boldsymbol{c}_{t-1}$, $\mathbf{W}_f$ is the weight of the forgetting gate, and $\mathbf{b}_f$ is the deviation of the forgetting gate, and the calculation formula is shown as follow:

$$\mathbf{f}_t = \sigma\left(\mathbf{W}_f \cdot [\mathbf{h}_{t-1}, \mathbf{x}_t] + \mathbf{b}_f\right) \tag{4}$$

The function tanh obtains the information of the candidate cell $\tilde{\mathbf{c}}_t$, and the calculation formula is written as

$$\tilde{\mathbf{c}}_t = \tanh(\mathbf{W}_c \cdot [\mathbf{h}_{t-1}, \mathbf{x}_t] + \mathbf{b}_c) \tag{5}$$

where $\mathbf{W}_c$ is the weight of the cell state, and $\mathbf{b}_c$ is the deviation of the cell state.

Updating the information of old cell $\mathbf{c}_{t-1}$ based on $\mathbf{i}_t$ and $\mathbf{h}_t$, can acquire the information of new cell $\mathbf{c}_t$, and the updating formula is shown as follow:

$$\mathbf{c}_t = \mathbf{i}_t \cdot \tilde{\mathbf{c}}_t + \mathbf{f}_t \cdot \mathbf{c}_{t-1} \tag{6}$$

The output gate $\mathbf{o}_t$ controls the output of information and the calculation formula is shown in Eq. (7). And at the moment of t, the calculation formula for the hidden layer $\mathbf{h}_t$ is shown in as follows:

$$\mathbf{o}_t = \sigma(\mathbf{W}_o \cdot [\mathbf{h}_{t-1}, \mathbf{x}_t] + \mathbf{b}_o) \tag{7}$$

$$\mathbf{h}_t = \mathbf{o}_t \cdot \tanh(\mathbf{c}_t) \tag{8}$$

where $\mathbf{W}_o$ and $\mathbf{b}_o$ represent the weight and bias of the output gate respectively.

LSTM improves the gradient disappearance or explosion problem that occurs in traditional RNNs due to its complex gated memory mechanism and outperforms other recurrent architectures in dealing with sequential tasks with long-term dependencies. However, it is worth noting that the LSTM structure can only use positive dependencies, and some useful information will be filtered in the long-term gated memory chain. In the process of picking FBs, the FBs at the current moment are correlated with the information before and after the current moment. In actual processing, we hope to deduce the FBs before and after the seismic trace from current FBs. To achieve the goal, this paper adopts the BiLSTM to better capture contextual long-term dependencies in sequence tasks and facilitate more precise predictions. Therefore, the current network model depends on both the previous and future FBs and their related information. Then, we propose the artificial intelligence regression approach based on BiLSTM to pick FBs in this paper.

2.5. Regression approach based on BiLSTM

BiLSTM is an improvement of LSTM, consisting of two LSTM layers in different directions, two independent LSTM layers, one for inputting the forward sequence and the other for inputting the reverse sequence. It combines the forward and backward hidden layers. The structure of the regression approach is based on BiLSTM as shown in Fig. 2. When dealing with timing issues, BiLSTM can better capture contextual long-term dependencies in sequence tasks and improve prediction accuracy. The regressive network architecture is composed of the input layer, the BiLSTM unit (including two independent LSTM layers and one LSTM hidden layer), the full collected layer (FC), the regression layer (regressor), and the output layer. Supposing in the shot gather there are n traces

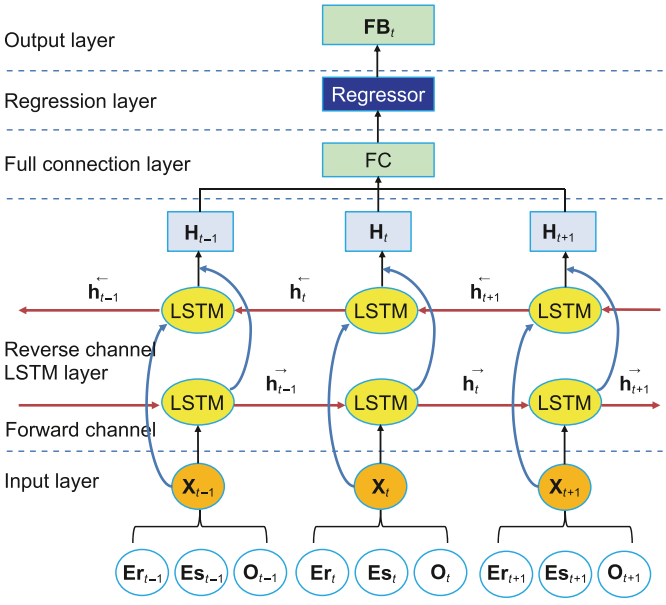

Fig. 2. The network structure of the BiLSTM based regressive model for picking FBs.

and m reliable labels which are made manually and by higher-order statistics based methods, noted as $\mathbf{FB}_j$ ($j = 1, 2, \ldots, m$). The elevation of the receiver, elevation of the shot and offset at the geophone point are denoted by $\mathbf{Er}_i$, $\mathbf{Es}_i$, and $\mathbf{O}_i$ ($j = 1, 2, \ldots, m$) respectively. In this method, the input layer is $\mathbf{X}$ which is a matrix consisting of $\mathbf{Er}_i$, $\mathbf{Es}_i$, and $\mathbf{O}_i$, and the output is $\mathbf{FB}$, which is a vector consisting of the FBs labels. Then we can create the nonlinear relationship mapping the observed variables in the field to the FBs through BiLSTM and FC. Taking the prediction of the FBs at the t-th seismic trace as an example, the forward LSTM and reverse LSTM output at t moment are $\overrightarrow{\mathbf{h}_t}$ and $\overleftarrow{\mathbf{h}_t}$, respectively.

In Fig. 2 and Eqs. (9) and (10), $\overrightarrow{\mathbf{h}_{t-1}}$, $\overrightarrow{\mathbf{h}_t}$, and $\overrightarrow{\mathbf{h}_{t+1}}$ represent the hidden layer neuron nodes model propagating forward; $\overleftarrow{\mathbf{h}_{t-1}}$, $\overleftarrow{\mathbf{h}_t}$, and $\overleftarrow{\mathbf{h}_{t+1}}$ represent the hidden layer neuron nodes propagating backward. The forward and backward implied state outputs of the BiLSTM are connected and fed into the same FC, and the output implied layer state is considered as input using the FC.

$$\overrightarrow{\mathbf{h}_t} = \mathrm{LSTM}\left(\overrightarrow{\mathbf{h}_{t-1}}, \mathbf{x}_t\right) \tag{9}$$

$$\overleftarrow{\mathbf{h}_t} = \mathrm{LSTM}\left(\overleftarrow{\mathbf{h}_{t+1}}, \mathbf{x}_t\right) \tag{10}$$

$$\mathbf{H}_t = \left[\overrightarrow{\mathbf{h}_t}, \overleftarrow{\mathbf{h}_t}\right] \tag{11}$$

The final FB estimated by the model at the time of t is

$$\mathbf{FB}_t = \mathbf{W}_\mathrm{F}\mathbf{H} + b_\mathrm{F} \tag{12}$$

where $\mathbf{H}$ represents the input of the FC, $\mathbf{W}_\mathrm{F}$ and b_F represent the weight matrix of the FC and the deviation of the output regression layer, respectively. In the BiLSTM networks, we have two groups of LSTM blocks, one as a backward layer and another as a forward layer, which provide two ways for transferring information: one from future to past and another from past to future. As a result, BiLSTM networks have a high ability in feature extraction and good performance in trace order to forecast traveltime.

After creating the framework to pick FBs, the training, evaluation, and application of the network model are further developed. The process of training network parameters can be considered as the process of constructing the implicit Eikonal equation using forward and reverse labels. In this paper, the quantitative outputs are continuous prediction values, instead of the two logical classification values of 0 and 1. The error between the predicted value and the label value at each trace affects the trained model. The difference between the network output and the label is evaluated by using the sum absolute error (SME) as Eq. (13) to make sure the predictions are approximate to each label in the training set. The SME can be calculated by

$$L = \sum_{j=1}^{m} \left| \mathrm{Regpicker}\left(\mathbf{Er}_j, \mathbf{Es}_j, \mathbf{O}_j, \boldsymbol{\theta}\right) - \mathbf{FB}_j \right| \tag{13}$$

The network is trained to minimize the loss L using adaptive moment estimation (Adam) (Kingma and Ba, 2014).The network weights $\boldsymbol{\theta}$ (a collection of $\mathbf{W}_\mathrm{F}$ and b_F, $\mathbf{W}_\mathrm{F}$ is initialized at random, and b_F is initialized to zero) in the network are updated as

$$\boldsymbol{\theta}_{k+1} = \boldsymbol{\theta}_k - \eta \nabla_{\boldsymbol{\theta}} L(\boldsymbol{\theta}) \tag{14}$$

where k is the iteration index, η is the learning rate, and $\nabla_{\boldsymbol{\theta}} L(\boldsymbol{\theta})$ is the gradient.

A set of labeled data sets (the validation set) is used to evaluate the network performance during the training. When the training loss decreases, whereas the validation loss increases (known as overfitting) or remains stable for a certain period of iterations, the training is stopped and the weights $\boldsymbol{\theta}_{\mathrm{opt}}$ are saved as the result of the training run. The saved optimal weights are used to predict the FBs on unseen data (or the testing set) with the following equation:

$$\overline{\mathbf{FB}_{\mathrm{test}}} = \mathrm{Regpicker}\left(\mathbf{Er}_{\mathrm{test}}, \mathbf{Es}_{\mathrm{test}}, \mathbf{O}_{\mathrm{test}}, \boldsymbol{\theta}_{\mathrm{opt}}\right) \tag{15}$$

3. Examples

The proposed method is tested on one model dataset and one land field dataset with low SNR. The flowchart of picking FBs based on the regressive model is shown in Fig. 3. The input data is the seismic data with the format of SEGY with geometry information. *PT* and *PV* denote the value of the proportion of the training set and the validation set in the label set, which is 0.75 and 0.25 respectively. The symbol *Itermax* means the maximum number of iterations, which is 4 in this paper. The symbol *Th0* means the maximum time error, which is defined as 10 ms. When the absolute error between predicted FB values and true FB values in the validation set is less than *Th0*, the regressive model trained by training set is considered effectively and can be used to predict the FBs of test set. Otherwise, it must retrain the regressive model after removing the training set data corresponding with the errors greater than 10 ms, and recreate the training set, the validation set, and the test set. By constructing the above-mentioned flowchart, the machine can make, optimize, and automatically reconstruct labels, with training and predicting FBs in a closed-loop environment. In each example, the number of hidden layers of the BiLSTM is 25, the initial learning rate is 0.008, the factor is reduced by 0.25 per 125 epochs, and the minimum learning rate is 0.001, the maximum number of epochs for training is assigned to 400, the sum absolute error is set to 0.001.

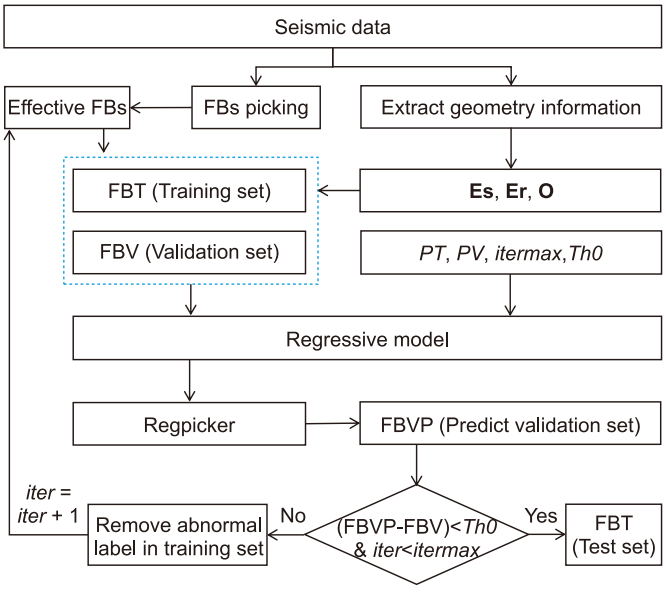

Fig. 3. Flowchart of picking FBs based on regressive model.

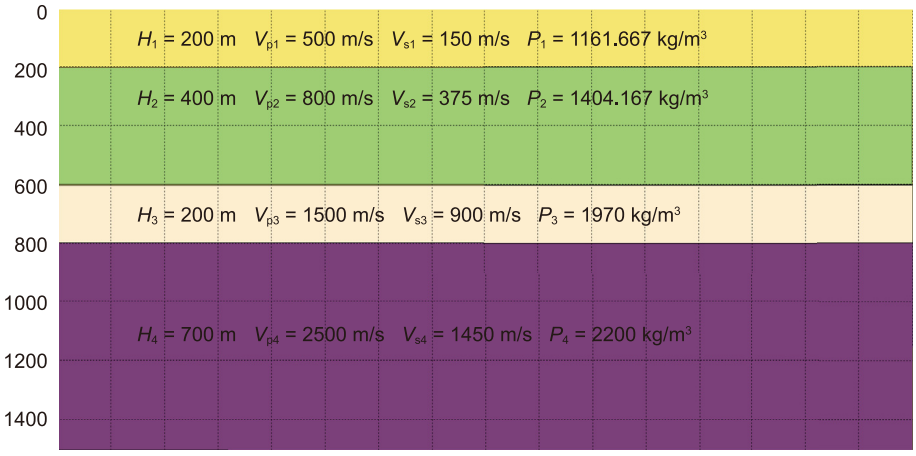

Fig. 4. The four-layer velocity model. H, V_p, V_s, and P in Fig. 4 represent the height, P-wave velocity, S-wave velocity, and density in each layer.

3.1. Test of numerical simulated data

The survey line is distributed along the horizontal surface, and shot points range from −200 m to 200 m, with an interval of 50 m. The receiver point distance is 25 m, evenly distributed along −4000 m to 4000 m, a total of 321 traces. A Ricker wavelet with a dominant frequency of 30 Hz with a length of 90 ms is used as the source, sampled at 2 ms and recorded for 5 s, simulating a total of 9 shots with 2989 traces. A four-layer velocity model is used in this section shown in Fig. 4. The total depth of the model is 1500 m. Depth of the four layers' bottom are 200, 600, 800 and 1500 m; P-wave velocity of the four layers are 500, 800, 1500, and 2500 m/s; S-wave velocity of the four layers are 150, 375, 900, and 1450 m/s; and density of the four layers are 1161.667, 1404.167, 1970 and 2200 kg/m^3. The numerical simulated data set is produced by elastic wave equations with mixed staggered-grid finite-difference schemes (Liu, et al., 2022).

Fig. 5 shows the 5th shot gather. From the shot gather we can see that, the first arrival wave includes a direct wave and a refracted wave, and two obvious refractive first arrival waves appear after 1.6 s, as shown by the red arrow in Fig. 5. The lateral amplitude changes obviously at the junction of the direct wave and the refractive first arrival wave, resulting in the first arrival wave waveform not clear, and brings great difficulties to identify and pick FBs.

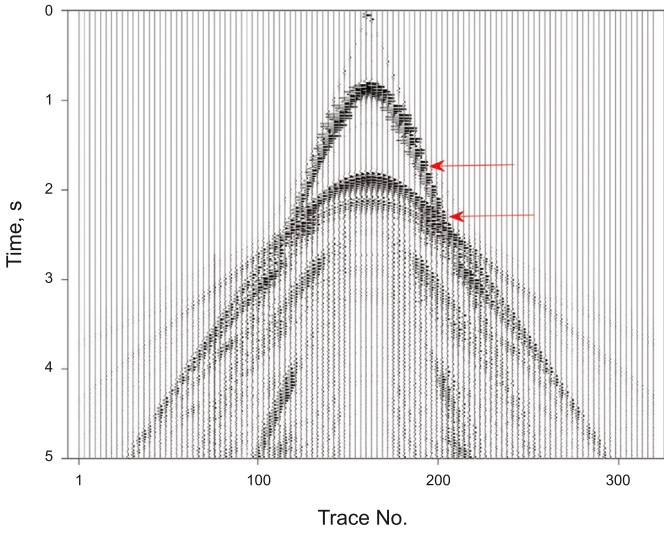

Fig. 5. The 5th shot gather.

The peaks of the first arrival waves are manually picked as the FBs of the seismic trace, and the label set is randomly selected to verify the method. The data are divided into three categories, the training set is composed of 644 traces (accounting for 22.3%), the validation set is composed of 199 traces (accounting for 6.7%), and the test set is composed of 2046 traces (accounting for 71%). Using the proposed method to conduct simulation tests. For the regressive network structure shown in Fig. 2, the input data is offset, the output is FBs, and map relationship is from offset to the FBs.

Seen from Fig. 6(a), the labels of FBs are continuous values between 0 and 3.7 s, with a minimum offset of 0 m and a maximum offset of 4200 m. The distribution of the predicted and true first arrival with offset for the training set, the validation set, and the test set is shown in Fig. 6(a)–(c) respectively. At the offset of 775 and 1550 m calculated by the least square linear fitting for FBs versus offset, the slope which responds to velocity for the FBs before and after it changes suddenly, and the entire first arrival curve can be divided into three segments with obvious differences. After optimal fitting, the three-segment velocities of the training set are 490.8, 796.4, and 2500 m/s, respectively. The three-segment velocities of the validation set are 494.5, 791.7, and 2500 m/s, respectively. The apparent velocities of the test set are 494.5, 791.7, and 2500 m/s, respectively. It can be seen that the network trained by this method has perfect generalization ability. The absolute error between the predicted and the true FBs of the training set, the validation set, and the test set are shown in Fig. 7(a)–(c), respectively.

From Fig. 7(a) we can see that the absolute error between the FBs predicted by the trained neural network and the true FBs in the training set is up to 4 ms, and the error of 639 samples is less than 4 ms, accounting for 99.22%. From Fig. 7(b) we can see that the absolute error between the FBs predicted by the trained neural network and the true FBs in the validation set is up to 4 ms, and the error of 198 samples is less than 4 ms, accounting for 99.5%. From Fig. 7(a) and (b), we can see that the neural network trained with randomly selected labels has good generalization ability, and can achieve relatively accurate picking results in both the training set and the validation set. Applying this network to the test data, the error is shown in Fig. 7(c), with a total of 1978 traces less than 4 ms, accounting for 96.68%. Therefore, we can conclude that the network trained by the label data accounting for 22.3% of all data, also has good prediction ability for the unknown seismic data, accounting for 71%.

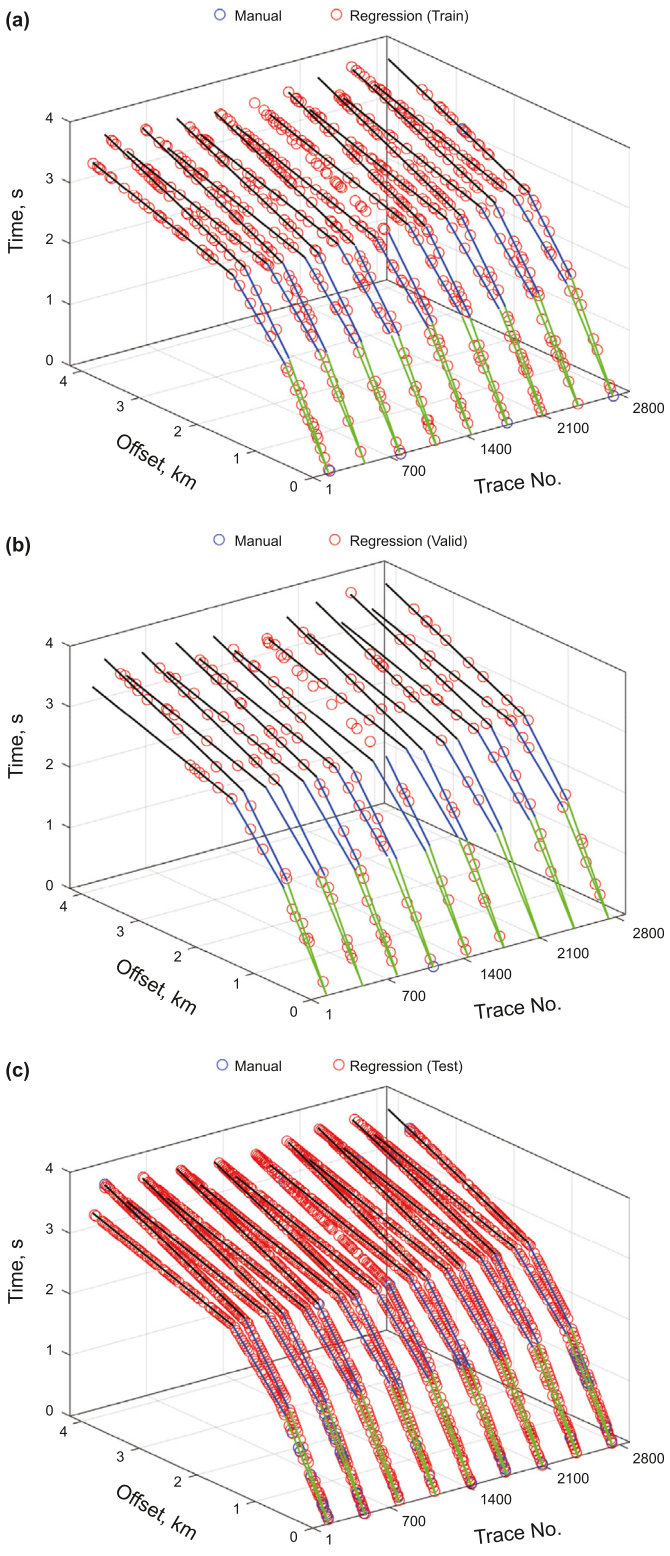

Fig. 6. FBs predicted by the proposed regression method and manually picked FBs in the training set (**a**), the validation set (**b**), and the test set (**c**), respectively.

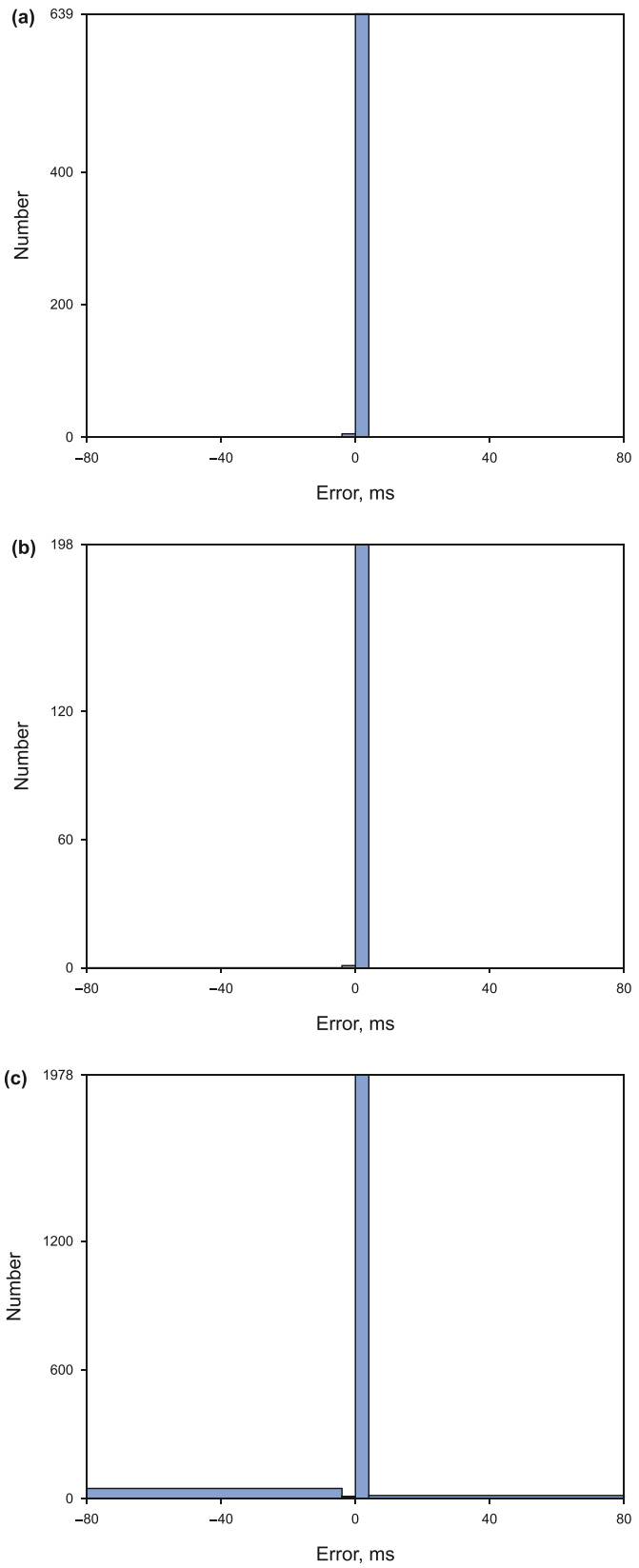

Fig. 7. Statistical errors of BiLSTM picked FBs in the training set (**a**), the validation set (**b**), and the test set (**c**), respectively.

To analyze the adaptability of this proposed method to the missing seismic data more clearly, we will analyze FBs predicted by the trained neural network of the 5th shot in details. The FBs of the

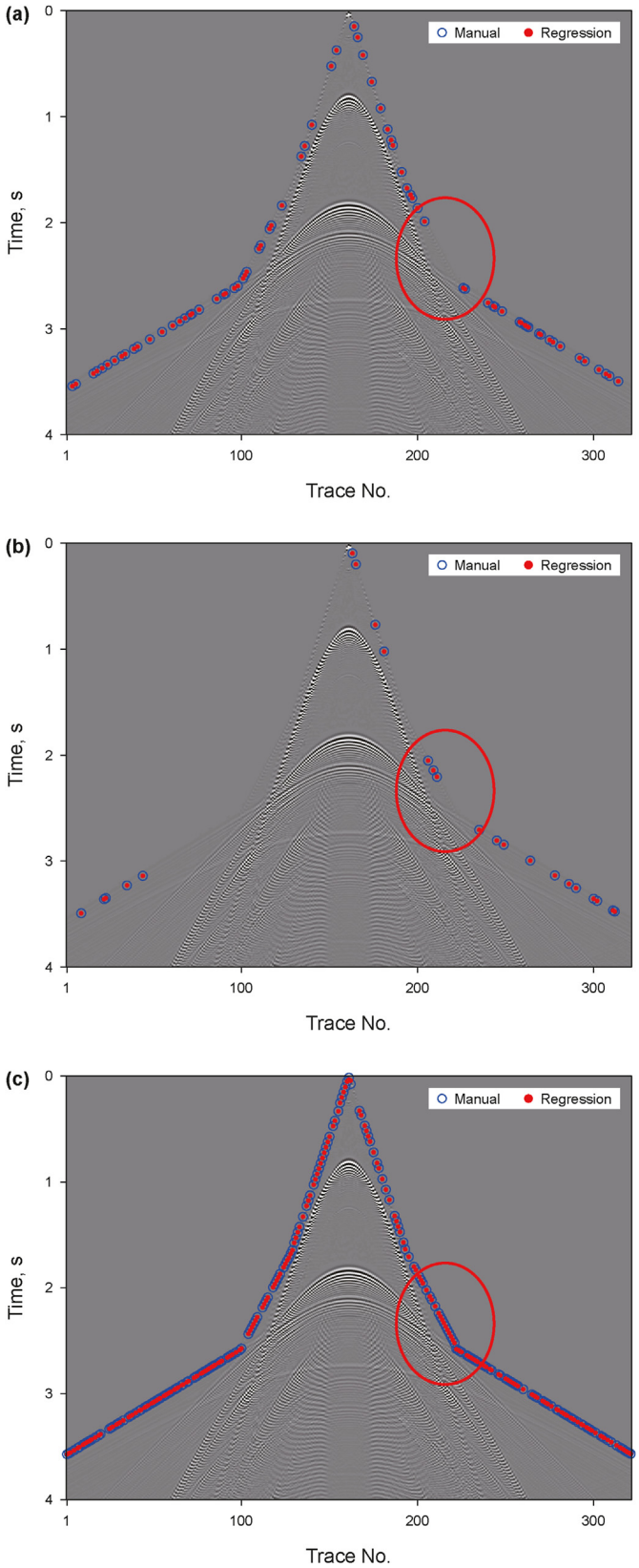

Fig. 8. Comparisons of manually picked FBs and FBs predicted by the proposed regression method in the training set (**a**), the validation set (**b**), and the test set (**c**) of the 5th shot gather, respectively.

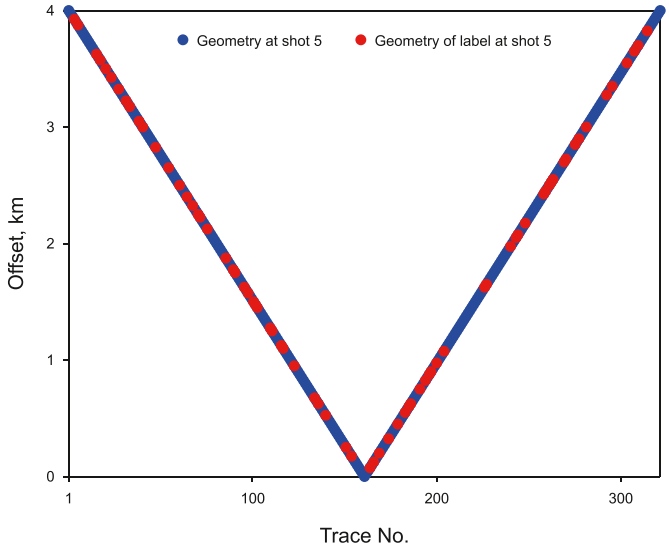

Fig. 9. Observation system information of the 5th shot gather.

training set and the 5th shot gather are shown in Fig. 8(a), from which we can see that the training set is randomly distributed with an obvious lack of traces, and the red circle indicates continuously missing 27 seismic traces which mainly correspond to the refracted wave at the third layer with a P-wave velocity of 1500 m/s and a thickness of 200 m. The FBs of the validation set and test set are shown in Fig. 8(b) and (c) respectively. As shown in Fig. 9, the blue points represent the offset information of the 5th shot gather, and the solid red circles represent the offset information of the label data set. From in Figs. 8 and 9, it can be seen that even if there is no label data corresponding to the refracted first arrival wave at the third layer in the training set, the distribution of first arrival in the local area in this shot can still be learned out perfectly by this method.

Through the above analysis, it can be seen that our method has obvious advantages in label production and training set construction, the trained network has strong generalization ability, and its predicted results of unknown seismic data have high accuracy and small error. In order to further verify the dependence of this regressive method on labels, in this paper we randomly select the second type of label data, training set consisted of 646 traces (accounting for 22.36%), the validation set consisted of 188 traces (accounting for 6.51%), and test set consisted of 2055 traces (accounting for 71.13%).

Shown in Fig. 10, the blue hollow circle represents the first type of label training set analyzed above, and the red points represent the second type of label training set. It can be seen from Fig. 10 that the two types of training sets selected randomly have great differences in location and distribution in shot gather, and both of them have random and continuous lack of seismic traces.

Fig. 11 shows the FBs are picked manually and predicted by the neural network trained based on the two types of label data sets. The blue circles represent the FBs predicted by the neural network trained by the first type of label data set, the red circles represent the FBs predicted based on the second type of label data set, and the black circles represent the FBs picked manually. It can be seen from Fig. 11 that the result predicted by this method is consistent with the trend of the FBs picked manually, and the values are almost

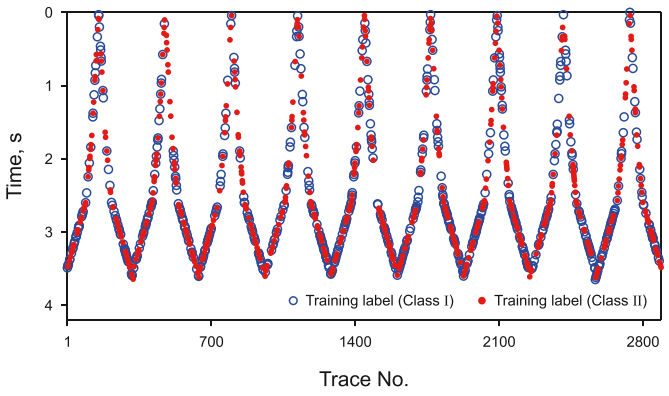

Fig. 10. FBs distributions of two types of training sets.

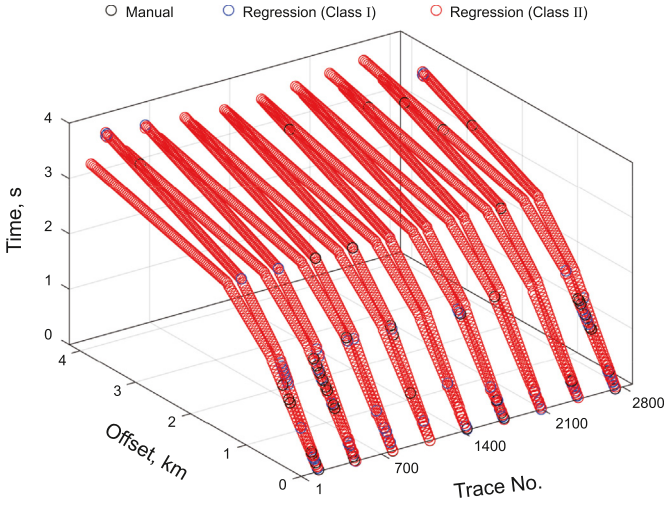

Fig. 11. FBs of two types of training sets.

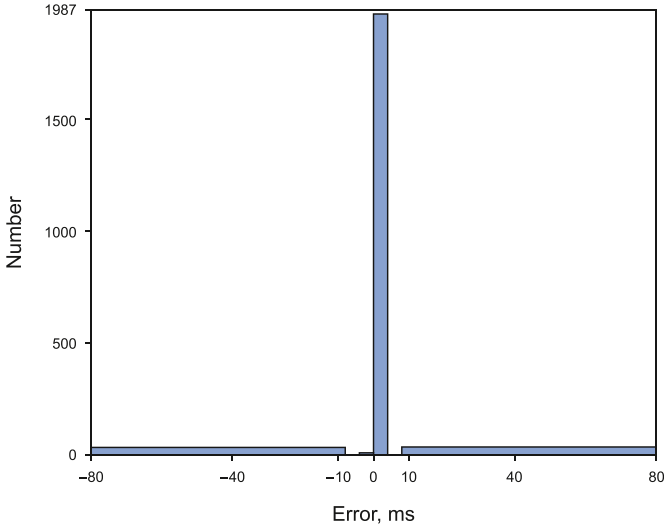

Fig. 12. Statistical errors of FBs predicted by the proposed regression neural network trained by the second type of label data set.

equal. Fig. 12 shows the error distribution of FBs predicted by the neural network trained with the second type of label data set, and there are 1987 traces with an error of less than 4 ms, accounting for 96.69%. That's to say the network trained with the second type of label data set can also precisely predict FBs, and also has good generalization ability.

According to the results of the above two types of randomly selected training set, validation set, and test set, it can be seen that even if there were large differences in the distribution and quantity of label data set, FBs can be predicted accurately for unknown seismic data. Therefore, our method has strong adaptability to random and continuous missing traces, and low dependence on labels. Even if large differences exist in the label data set, a relatively accurate implicit regressive model that characterizes the relationship between the information of geometry and FBs can be trained to predict FBs perfectly. This advantage provides a good foundation for industrial application of picking FBs based on artificial intelligence methods.

3.2. Test of low SNR field seismic data

There are a total of 9380 common-shot gathers and 4209709 traces in this area. The surface is relatively gentle, and the surface elevation ranges between 460 m and 680 m with the terrain high in the south and low in the north. The source elevation and geophone elevation of the area are shown in Fig. 13(a) and (b) respectively. The seismic data in this area are excited by a vibrator source, and the SNR of seismic data are relatively low. The amplitude of the first arrival wave in the shot gather is weak, and the spatial consistency of the waveform is poor. In addition, scattering waves, surface waves, and other noise interference are widely existed, which brings great trouble to picking FBs. Fig. 14 gives two typical shot gathers in this area. According to the method provided in this paper, the model is retrained and the FBs are picked in the whole work area.

In the field data, we introduce the proportion of three data sets as a whole seen detailed in Table 1, and the training set is composed of 712779 traces (accounting for 16.93%), the validation set is composed of 237593 traces (accounting for 5.64%), and the test set is composed of 3259337 traces (accounting for 77.43%). The total cost time of picking FBs by commercial software is 763 min in the entire process, while it takes 143 min to pick FBs using the presented method in this paper, more details seen in Table 2. From Table 1, we can see that the numbers of FBs edited manually after picking used commercial software and only through the presented method are 2432501 (accounting for 57.78%) and 3959876 (accounting for 94.07%) respectively. As can be seen from Table 2 and it spends most of the time on pre-processing (accounting for 36.17%) and post-processing (accounting for 52.69%) using commercial software, while it spends most of the time focusing on model training (accounting for 79.02%) used presented method. It is needed to remind that other elapsed time, such as reading and writing seismic data, is incorporated into label creation and test set data prediction respectively. From the two tables, it can be concluded that it takes less time with more efficiency and less manpower to use the presented method than using commercial software.

A prevalent commercial software and the proposed method are separately used to pick FBs of the whole area, and the results of FBs versus offset are shown in Fig. 15(a) and (b), respectively. The main strategy of the commercial software is to manually pick part of the shot gathers as a seed shot, and then use the prior information of the seed shot to extract the sensitive attribute parameters corresponding to the first arrival wave to automatically pick FBs among whole seismic data in the work area. In the tomographic inversion static correction technology based on FBs, the information of FBs with small offset is very important in inverting the surface and shallow velocity model, and also has a great influence on the

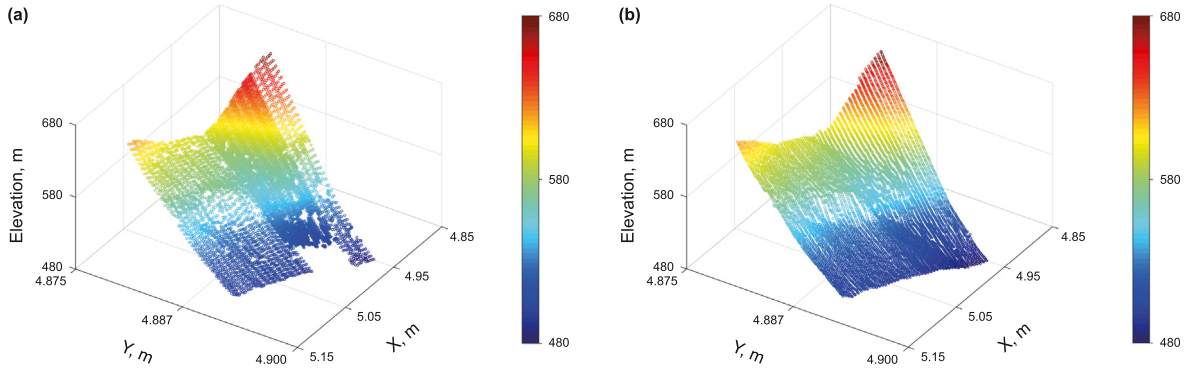

Fig. 13. Elevations of source points **(a)** and receiver points **(b)**, respectively.

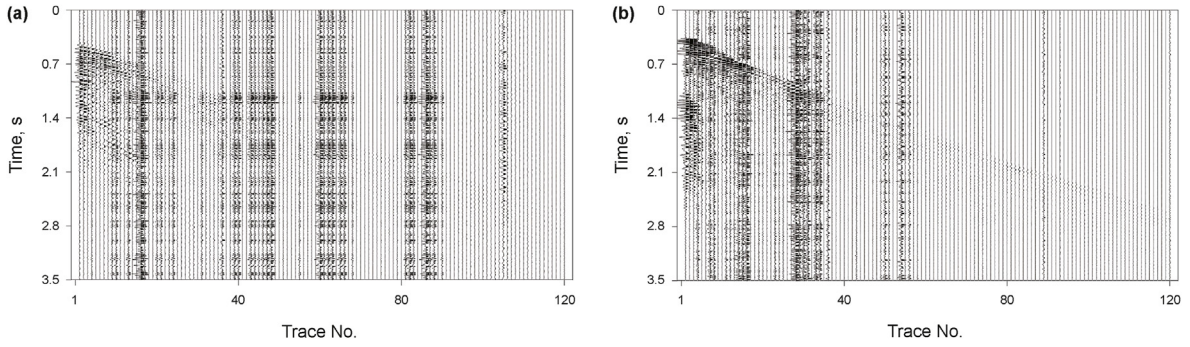

Fig. 14. Two typical shot gathers in the working area.

Table 1
Data information and processing result in two cases.

Method	Total shot number	Total trace number	Picked FBs number	Total time, min
Commercial software	9380	4209709	2432501	763
Regression method			3959876	143

Table 2
Running time in two cases.

Commercial software			Regression method					
Pre-process time, min	Auto picking time, min	Post-process time, min	Label set		Training set		Validation set	
			Number	Time, min	Number	Time, min	Number	Time, min
276	85	402	–	–	–	–	–	–
–	–	–	950372	14	712779	113	237593	16

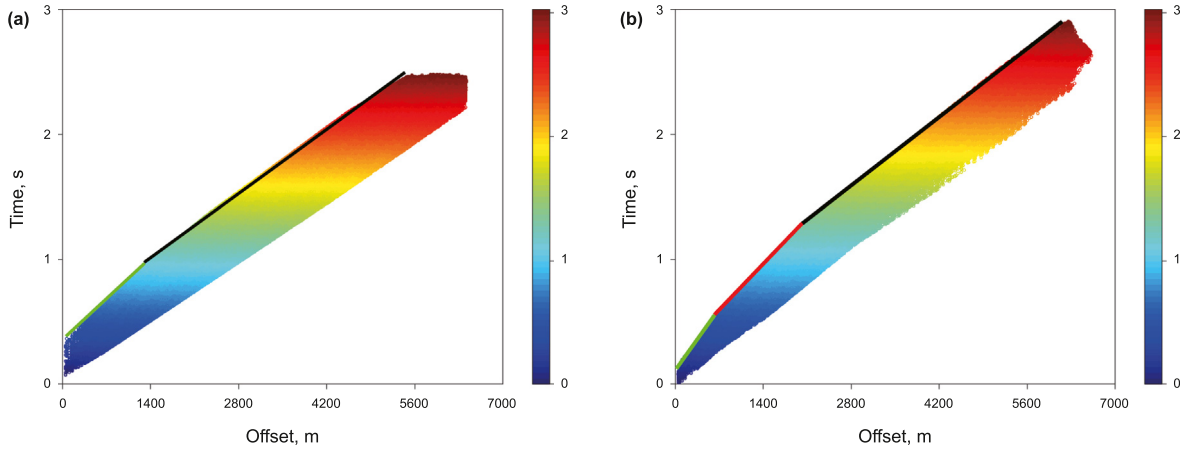

Fig. 15. FBs picked by commercial software **(a)** and the proposed regression method **(b)**, respectively.

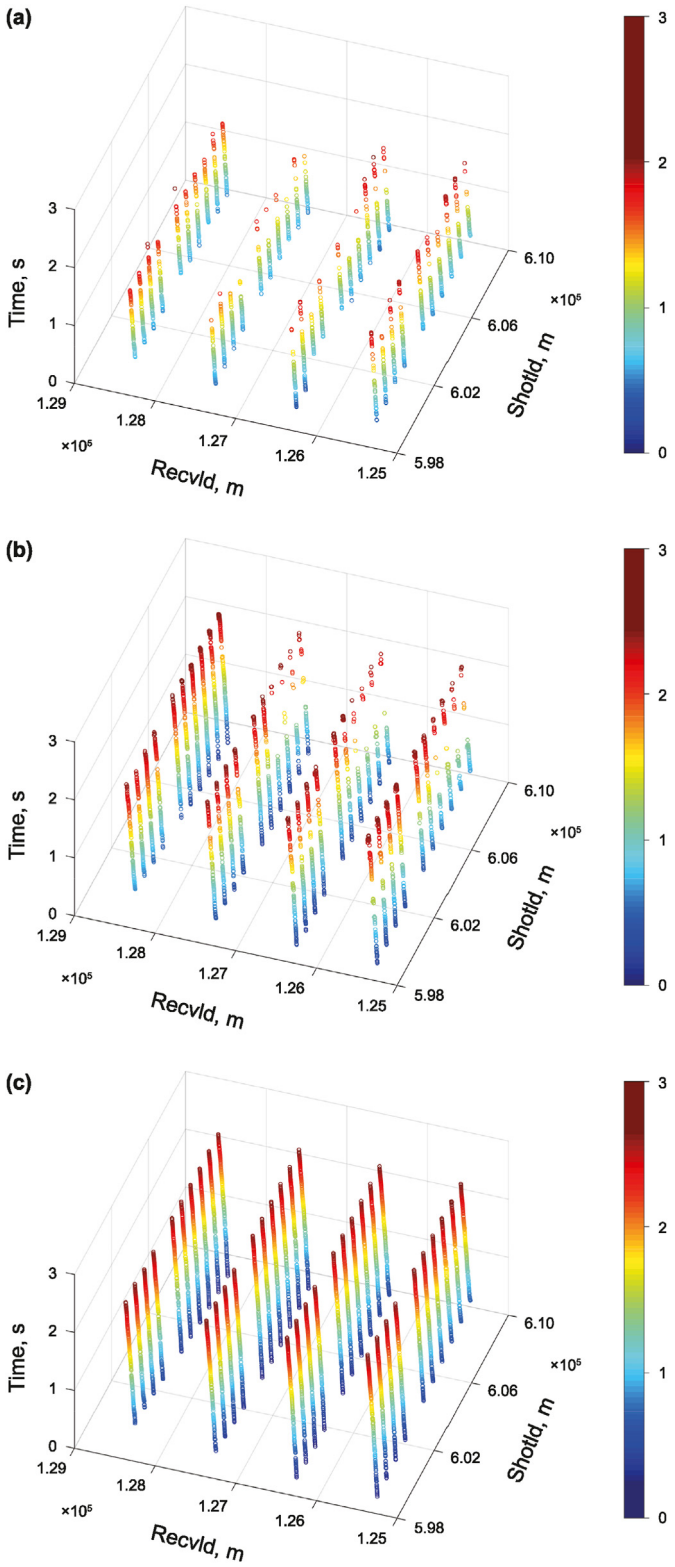

Fig. 16. Comparisons of FBs of shot ID282–391 picked by different methods. **(a)** FBs labels, **(b)** FBs picked by the conventional commercial software, **(c)** FBs picked by our regression method. In each subfigure, the symbols Recvld, Shotld and Time represent the receiver point position, the shot point position, and the first arrival time, respectively.

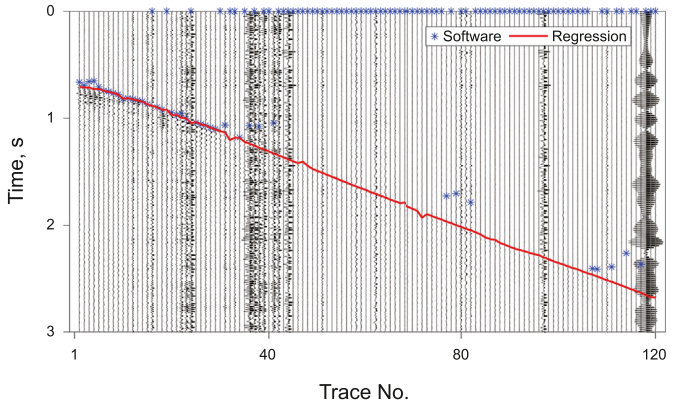

Fig. 17. First arrival of shot ID282 picked by a popular commercial software (blue asterisks) and our regression method (the red line).

quality of the medium and deep imaging. From Fig. 15, we can see that FBs picked by our method have better focus and consistency within the same offset range than those picked by commercial software. Along the upper boundary of the FBs, compared with Fig. 15(a), there are two clear inflection points at an offset of 550 and 1000 m in Fig. 15(b). It can also be seen that the FBs are divided into three obvious segments which correspond to the three layers of the geological model, and the three slope values represent the apparent slowness values for each layer. The reciprocal of these three apparent slowness values as the initial velocity for tomography inversion can not only improve the inversion efficiency, but also improve the inversion accuracy of the velocity model. The maximum FBs in Fig. 15(a) is less than 2.5 s and the maximum value in Fig. 15(b) is about 2.9 s, which indicates that there is a huge difference in the accuracy of FBs and the range of larger offset successfully picked FBs by the proposed method. Generally, under conditions of accurate FBs, the bigger the FBs corresponding to the far offset, the stronger the ability to depict the deep velocity model.

To further study the reliability and accuracy of the proposed method, a total of 10 shots with ID382–391 containing 4800 seismic traces are extracted for fine comparison. Fig. 16(a) represents the FBs label data set for the proposed method, and Fig. 16(b) and (c) give the results picked by commercial software and our artificial intelligence regressive method respectively. The label data set in Fig. 16(a) composed of randomly selected 1857 traces, accounting for 33.06%, which distributes non-uniformly, especially lack of the middle and far offset labels. Fig. 16(b) gives the FBs picked by commercial software, and only randomly distributed 2803 traces' FBs, rarely existing in middle and far offset. The result picked by our method is shown in Fig. 16(c), and all seismic traces can be picked even if lack middle-far offset labels. Fig. 17 gives the FBs of one shot with ID382, the blue asterisks and the red line respectively represent the FBs picked by commercial software and those picked by our method. As can be seen from Fig. 17, there is serious noise in the shot data with low SNR and poor lateral consistency of the seismic waveform. The FBs picked by commercial software are concentrated on the near offset, accompanied with low pick-up rate and poor precision with sparse FBs distributed in middle-far offsets. However, the result predicted by the proposed regressive method is perfect, accompany with high enough and accurate FBs ranging from near-offset to mid-far-offset. Comparing Figs. 16 and 17, it can be seen that the FBs picked by the proposed

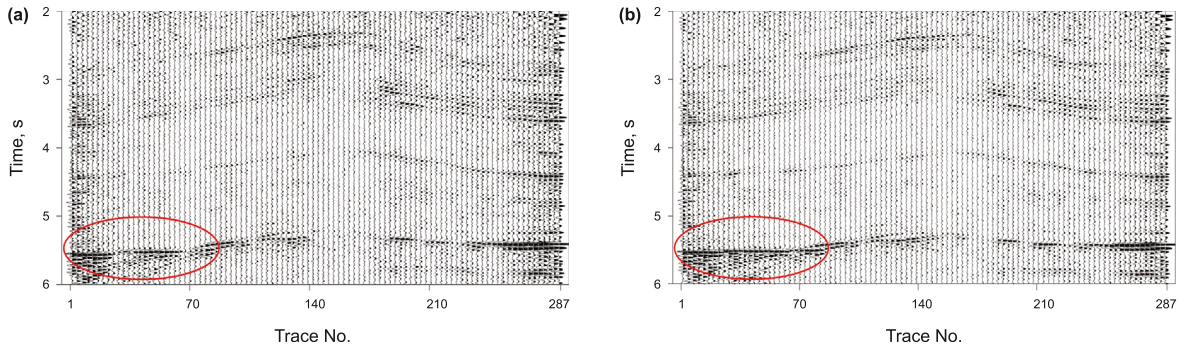

Fig. 18. Stacked profiles with static correction based on FBs picked by commercial software **(a)** and the proposed regression method **(b)**, respectively.

method are much higher than those picked by the commercial software in terms of accuracy and pick-up rate.

To get static correction calculated with the tomography inversion method based on FBs using the conventional commercial software following the same parameters and process flow. A main survey line is extracted from the 3D seismic area, and we will use the image quality of the stacked profiles to evaluate the quality of the FBs. The same stack velocity is used to superimpose each of them and analyze the imaging. Fig. 18(a) and (b) respectively gives the stacked profile with static correction. Comparing Fig. 16(a) with Fig. 16(b), we can see that, from the shallow to the deep, the stack profile given in Fig. 18(b) has better transverse continuity in seismic events with higher SNR. Moreover, due to the higher picking quality and higher picking density of the far-offset seismic traces in this method, the deep event around 5.5 s (indicated by the red circle) in Fig. 18(b) has obviously better imaging quality.

4. Conclusions

In this paper, a regressive artificial intelligence FBs picking method is proposed to overcome the shortcomings of the DL method based on image segmentation in recent years, which is difficult to apply in seismic data with low SNR and is difficult to balance the picking efficiency and accuracy.

It is difficult and inefficient to make regular seismic image labels with the same size in massive seismic data, and this end-to-end input mode greatly limits the practicality of DL technology based on image segmentation for first arrival picking. The input of our method is a vector composed of the known seismic observation information, and the output is the FBs of the seismic trace. Only a part of the sparsely accurate FBs are selected for network training, which greatly reduces the difficulty for label production, circumvents the high requirements for seismic data quality, and improves the adaptability of artificial intelligence technology to pick FBs.

The label data set of our method is composed of randomly distributed seismic traces' first arrival time, which does not need to be one-size and regular high-dimensional label. A part of the FBs picked by traditional automatic or manual picking method can be used as a label, so the label production is more flexible, convenient, and fast, which provides favorable conditions for our regressive artificial intelligence approach for picking FBs to realize industrialization.

The model data test shows that the two label data sets with different distributions, quantity, and location can finally obtain satisfactory and similar results, which indicates that the dependence of our method on the label data set is very low.

The test of 3D field seismic data with low SNR shows that the operation process of our method is simple and easy, without cumbersome preprocessing work, and the picking results are rarely affected by the quality of seismic data. Even though the seismic data with low SNR and irregular acquisition, the accuracy of FBs and pick-up rate are very high, and the subsequent imaging quality is very good. Thus our method has good application effectiveness and promotion value.

The trained neural network model based on the proposed method in this paper is only suitable for the data of the work area itself and cannot be directly applied to other work areas, which reduces the operation efficiency of this method in field data. In the follow-up research, it is necessary to further study the transfer learning technology and optimize the trained deep learning network after optimizing the label data or changing the areas, so that it can be directly and quickly generalized to the new work area with high efficiency.

Declaration of competing interest

The authors declare that they have no known competing financial interests or personal relationships that could have appeared to influence the work reported in this paper.

Acknowledgements

This work was financially supported by the National Key R&D Program of China (2018YFA0702504), the National Natural Science Foundation of China (42174152), the Strategic Cooperation Technology Projects of China National Petroleum Corporation (CNPC) and China University of Petroleum-Beijing (CUPB) (ZLZX2020-03), and the R&D Department of China National Petroleum Corporation (2022DQ0604-01).

References

Akram, J., Eaton, D., 2016. A review and appraisal of arrival-time picking methods for downhole microseismic data. Geophysics 81 (2), KS71–KS91. https://doi.org/10.1190/geo2014-0500.1.

Badrinarayanan, V., Kendall, A., Cipolla, R., 2017. SegNet: a deep convolutional encoder-decoder architecture for image segmentation. IEEE Trans. Pattern Anal. Mach. Intell. 39 (12), 2481–2495. https://doi.org/10.1109/TPAMI.2016.2644615.

Boschetti, F., Dentith, M.D., List, R., 1996. A fractal-based algorithm for detecting first arrivals on seismic traces. Geophysics 61, 1095–1102. https://doi.org/10.1190/1.1444030.

Chen, D., Yang, W., Wei, X.J., et al., 2020. Aoutomatic picking of seismic first arrival based on hybrid network U-SegNet. Oil Geophys. Prospect. 55 (6), 1188–1201 (in Chinese).

Chen, L., Papandreou, G., Kokkinos, I., et al., 2018. Deeplab: semantic image segmentation with deep convolutional nets, atrous convolution, and fully connected CRFs. IEEE T Pattern Anal. 40 (4), 834–848. https://doi.org/10.1109/TPAMI.2017.2699184.

Coppens, F., 1985. First arrival picking on common-offset trace collections for automatic estimation of static corrections. Geophys. Prospect. 33, 1212–1231. https://doi.org/10.1111/j.1365-2478.1985.tb01360.x.

David, C., Liu, Y., Ding, C.Z., et al., 2021. First break picking method based on artificial intelligence and apparent velocity. Oil Geophys. Prospect. 56 (3), 419–435 (in

Chinese).
Duan, X., Zhang, J., 2020. Multi-trace first break picking using an integrated seismic and machine learning method. Geophysics 85 (4), WA269–WA277. https://doi.org/10.1190/geo2019-0422.1.
Gaci, S., 2014. The use of wavelet-based denoising techniques to enhance the first-arrival picking on seismic traces. IEEE Trans. Geosci. Rem. Sens. 52, 4558–4563. https://doi.org/10.1109/TGRS.2013.2282422.
Gelchinsky, B., Shtivelman, V., 1983. Automatic picking of the first arrival and parameterization of traveltime curves. Geophys. Prospect. 31, 915–928. https://doi.org/10.1111/j.1365-2478.1983.tb01097.x.
Gentili, S., Michelini, A., 2006. Automatic picking of P and S phases using a neural tree. J. Seismol. 10 (1), 39–63. https://doi.org/10.1007/s10950-006-2296-6.
Gibbons, S., Ringdal, F., 2006. The detection of low magnitude seismic events using array-based waveform correlation. Geophys. J. Int. 165 (1), 149–166. https://doi.org/10.1111/j.1365-246X.2006.02865.x.
Han, S., Liu, Y., Li, Y., et al., 2021. First arrival traveltime picking through 3-D U-Net. IEEE Geosci. Remote Sens. Lett. 19, 1–5. https://doi.org/10.1190/geo2018-0688.1.
Hu, L., Zheng, X., Duan, Y., et al., 2019. First-arrival picking with a U-net convolutional network. Geophysics 84 (6), U45–U57. https://doi.org/10.1190/geo2018-0688.1.
Jiao, L., Moon, W., 2000. Detection of seismic refraction signals using a variance fractal dimension technique. Geophysics 65, 286–292. https://doi.org/10.1190/1.1444719.
Khalaf, A., Camerlynck, C., Florsch, N., et al., 2018. Development of an adaptive multi-method algorithm for automatic picking of first arrival times: application to near surface seismic data. Near Surf. Geophys. 16 (5), 507–526. https://doi.org/10.1002/nsg.12014.
Kingma, D., Ba, J., 2014. Adam: a method for stochastic optimization. ArXiv preprint arXiv:1412.6980.
Li, J., Tang, S., Li, K., et al., 2022. Automatic recognition and classification of microseismic waveforms based on computer vision. Tunn. Undergr. Space Technol. 121, 104327. https://doi.org/10.1016/j.tust.2021.104327.
Li, J., Li, K., Tang, S., 2023. Automatic arrival-time picking of P- and S-waves of microseismic events based on object detection and CNN. Soil Dynam. Earthq. Eng. 164, 107560. https://doi.org/10.1016/j.soildyn.2022.107560.
Liu, W., Hu, Z., Yong, X., et al., 2022. Wave equation numerical and RTM with mixed staggered-finite-difference schemes. Front. Earth Sci. 10, 873541. https://doi.org/10.3389/feart.2022.873541.
Maity, D., Aminzadeh, F., Karrenbach, M., 2014. Novel hybrid artificial neural network based autopicking workflow for passive seismic data. Geophys. Prospect. 62 (4), 834–847. https://doi.org/10.1111/1365-2478.12125.
McCormack, M., Zaucha, D., Dushek, D., 1993. First-break refraction event picking and seismic data trace editing using neural networks. Geophysics 58, 67–78. https://doi.org/10.1190/1.1443352.
Molyneux, J., Schmitt, D., 1999. First-break timing: arrival onset times by direct correlation. Geophysics 64, 1492–1501. https://doi.org/10.1190/1.1444653.
Noack, M., Clark, S., 2017. Acoustic wave and eikonal equations in a transformed metric space for various types of anisotropy. Heliyon 3 (3), 122. https://doi.org/10.1016/j.heliyon.2017.e00260.
Noh, H., Hong, S., Han, B., 2015. Learning deconvolution network for semantic segmentation. In: ICCV, pp. 1520–1528. https://doi.org/10.1109/ICCV.2015.178.
Ronneberger, O., Fischer, P., Brox, T., 2015. U-net: convolutional networks for biomedical image segmentation. arXiv preprint. https://doi.org/10.1007/978-3-319-24574-4_28.
Sabbione, J., Velis, D., 2010. Automatic first-breaks picking: new strategies and algorithms. Geophysics 75 (4), 67–76. https://doi.org/10.1190/1.3463703.
Saragiotis, C., Hadjileontiadis, L., Rekanos, I., et al., 2004. Automatic P phase picking using maximum kurtosis and k-statistics criteria. Geosci. Rem. Sens. Lett. IEEE 1, 147–151. https://doi.org/10.1109/LGRS.2004.828915.
Saxe, A., McClelland, J., Ganguli, S., Exact solutions to the nonlinear dynamics of learning in deep linear neural networks. arXiv preprint, arXiv:1312.6120..
Sleeman, R., Eck, T., 1999. Robust automatic P-phase picking: an online implementation in the analysis of broadband seismogram recordings. Phys Earth Planet Inter. 113, 265–275. https://doi.org/10.1016/S0031-9201(99)00007-2.
Takanami, T., Kitagawa, G., 1991. Estimation of the arrival times of seismic waves by multivariate time series mode1. Ann. Inst. Stat. Math. 43 (3), 407–433. https://doi.org/10.1007/BF00053364.
Takanami, T., Kitagawa, G., 1993. Multivariate time-series model to estimate the arrival times of S-waves. Comput. Geosci. 19 (2), 295–301.
Tsai, K., Hu, W., Wu, X., et al., 2020. Automatic first arrival picking via deep learning with human interactive learning. IEEE Trans. Geosci. Rem. Sens. 58 (2), 1380–1391. https://doi.org/10.1109/TGRS.2019.2946118.
Tselentis, G., Martakis, N., Paraskevopoulos, P., et al., 2012. Strategy for automated analysis of passive microseismic data based on S-transform, Otsu's thresholding, and higher order statistics. Geophysics 77 (6), 43–54. https://doi.org/10.1190/GEO2011-0301.1.
Yilmaz, O., 2001. Seismic Data Analysis: Processing, Inversion, and Interpretation of Seismic Data. Society of Exploration Geophysicists. https://doi.org/10.1190/1.9781560801580.
Yuan, S., Liu, J., Wang, S., et al., 2018. Seismic waveform classification and first-break picking using convolution neural networks. Geosci. Rem. Sens. Lett. IEEE 15 (2), 272–276. https://doi.org/10.1109/LGRS.2017.2785834.
Yuan, S., Zhao, Y., Xie, T., et al., 2022. SegNet-based first-break picking via seismic waveform classification directly from shot gathers with sparsely distributed traces. Petrol. Sci. 19 (1), 162–179. https://doi.org/10.1016/j.petsci.2021.10.010.
Yung, S., Ikelle, L., 1997. An example of seismic time-picking by third-order bicoherence. Geophysics 62, 1947–1952. https://doi.org/10.1190/1.1444295.
Zhang, J., Sheng, G., 2020. First arrival picking of microseismic signals based on nested U-Net and Wasserstein Generative Adversarial Network. J. Pet. Sci. Eng. 195, 107527. https://doi.org/10.1016/j.petrol.2020.107527.
Zhao, M., Chen, S., Fang, L., et al., 2019. Earthquake phase arrival auto-picking based on U-shaped convolutional neural network. Chin. J. Geophys. 62 (8), 3034–3042. https://doi.org/10.6038/cjg2019M0495 (in Chinese).